REPORT DOCUMENTATION PAGE

Form Approved OMB NO. 0704-0188

1. REPORT DATE (DD-MM-YYYY)	2. REPORT TYPE	3. DATES COVERED (From - To)
	New Reprint	-

4. TITLE AND SUBTITLE
Anion Transport in a Chemically Stable, Sterically Bulky ?-C Modified Imidazolium Functionalized Anion Exchange Membrane

5a. CONTRACT NUMBER
W911NF-10-1-0520

5b. GRANT NUMBER

5c. PROGRAM ELEMENT NUMBER
611103

6. AUTHORS
Ye Liu, Junhua Wang, Yuan Yang, Thomas M. Brenner, Söenke Seifert, Yushan Yan, Matthew W. Liberatore, Andrew M. Herring

5d. PROJECT NUMBER

5e. TASK NUMBER

5f. WORK UNIT NUMBER

7. PERFORMING ORGANIZATION NAMES AND ADDRESSES
Colorado School of Mines
1500 Illinois St

Golden, CO 80401 -1911

8. PERFORMING ORGANIZATION REPORT NUMBER

9. SPONSORING/MONITORING AGENCY NAME(S) AND ADDRESS (ES)
U.S. Army Research Office
P.O. Box 12211
Research Triangle Park, NC 27709-2211

10. SPONSOR/MONITOR'S ACRONYM(S)
ARO

11. SPONSOR/MONITOR'S REPORT NUMBER(S)
58161-CH-MUR.52

12. DISTRIBUTION AVAILIBILITY STATEMENT
Approved for public release; distribution is unlimited.

13. SUPPLEMENTARY NOTES
The views, opinions and/or findings contained in this report are those of the author(s) and should not contrued as an official Department of the Army position, policy or decision, unless so designated by other documentation.

14. ABSTRACT
The morphology and anion transport of an ?-C modified imidazolium functionalized anion exchange membrane, 1,4,5-trimethyl-2-(2,4,6-trimethoxyphenyl)imidazolium functionalized polyphenylene oxide (with ion exchange capacity {IEC} = 1.53 or 1.82 mequiv/g), were studied in detail. The novel cation is less susceptible to OH– attack (0% degradation) compared to unsubstituted imidazolium functionalized polyphenylene oxide (25% degradation) after 24 h at 80 °C in 1 M KOH. The two different IEC materials (with the same protected cation) show interesting differences in membrane performance. From AFM and SAXS under humid conditions, the domain sizes of the

15. SUBJECT TERMS
Anion Exchange Membrane, stable cation, anion transport, morphology

16. SECURITY CLASSIFICATION OF:			17. LIMITATION OF ABSTRACT	15. NUMBER OF PAGES	19a. NAME OF RESPONSIBLE PERSON
a. REPORT	b. ABSTRACT	c. THIS PAGE			Andrew Herring
UU	UU	UU	UU		19b. TELEPHONE NUMBER: 303-384-2082

Report Title

Anion Transport in a Chemically Stable, Sterically Bulky ?-C Modified Imidazolium Functionalized Anion Exchange Membrane

ABSTRACT

The morphology and anion transport of an ?-C modified imidazolium functionalized anion exchange membrane, 1,4,5-trimethyl-2-(2,4,6-trimethoxyphenyl)imidazolium functionalized polyphenylene oxide (with ion exchange capacity {IEC} = 1.53 or 1.82 mequiv/g), were studied in detail. The novel cation is less susceptible to OH– attack (0% degradation) compared to unsubstituted imidazolium functionalized polyphenylene oxide (25% degradation) after 24 h at 80 °C in 1 M KOH. The two different IEC materials (with the same protected cation) show interesting differences in membrane performance. From AFM and SAXS under humid conditions, the domain sizes of the membrane change, which impact the transport properties. The lower IEC sample showed a smaller tortuosity and, thus, needs a longer diffusion time for the water molecules to be fully hindered inside the hydrophobic clusters, which is confirmed by water self-diffusion measurements from pulsed field gradient NMR. From conductivity and diffusion measurements, the higher IEC sample exhibited Vogel–Tammann–Fulcher behavior, thus indicating that the polymer chain's movement dominates the transport. However, the lower IEC sample exhibited the linear Arrhenius behavior signifying water-mediated transport. The maximum Cl– conductivity observed was 23 mS/cm at 95% RH and 90 °C.

REPORT DOCUMENTATION PAGE (SF298)
(Continuation Sheet)

Continuation for Block 13

ARO Report Number 58161.52-CH-MUR
Anion Transport in a Chemically Stable, Sterical...

Block 13: Supplementary Note

Approved for public release; distribution is unlimited.

THE JOURNAL OF PHYSICAL CHEMISTRY C

Article

pubs.acs.org/JPCC

Anion Transport in a Chemically Stable, Sterically Bulky α-C Modified Imidazolium Functionalized Anion Exchange Membrane

Ye Liu,[†] Junhua Wang,[‡] Yuan Yang,[§] Thomas M. Brenner,[∥] Söenke Seifert,[⊥] Yushan Yan,[‡] Matthew W. Liberatore,[†] and Andrew M. Herring*[,†]

[†]Department of Chemical and Biological Engineering, [§]Department of Chemistry and Geochemistry, and [∥]Department of Physics, Colorado School of Mines, Golden, Colorado 80401, United States

[‡]Department of Chemical and Biomolecular Engineering, University of Delaware, Newark, Delaware 19716, United States

[⊥]X- Ray Science Division, Argonne National Laboratory, Argonne, Illinois 60439, United States

Supporting Information

ABSTRACT: The morphology and anion transport of an α-C modified imidazolium functionalized anion exchange membrane, 1,4,5-trimethyl-2-(2,4,6-trimethoxyphenyl)imidazolium functionalized polyphenylene oxide (with ion exchange capacity {IEC} = 1.53 or 1.82 mequiv/g), were studied in detail. The novel cation is less susceptible to OH^- attack (0% degradation) compared to unsubstituted imidazolium functionalized polyphenylene oxide (25% degradation) after 24 h at 80 °C in 1 M KOH. The two different IEC materials (with the same protected cation) show interesting differences in membrane performance. From AFM and SAXS under humid conditions, the domain sizes of the membrane change, which impact the transport properties. The lower IEC sample showed a smaller tortuosity and, thus, needs a longer diffusion time for the water molecules to be fully hindered inside the hydrophobic clusters, which is confirmed by water self-diffusion measurements from pulsed field gradient NMR. From conductivity and diffusion measurements, the higher IEC sample exhibited Vogel−Tammann−Fulcher behavior, thus indicating that the polymer chain's movement dominates the transport. However, the lower IEC sample exhibited the linear Arrhenius behavior signifying water-mediated transport. The maximum Cl^- conductivity observed was 23 mS/cm at 95% RH and 90 °C.

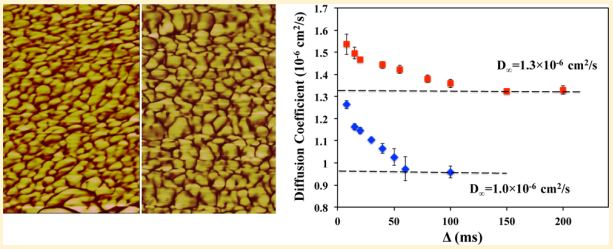

1. INTRODUCTION

Advanced anion exchange membranes (AEMs) have the potential to enable new electrochemical devices based on catalysis in alkaline media such as fuel cells or electrolyzers.[2] However, little is known about transport in these newer materials.[3] Alkaline fuel cells (AFCs) have been widely investigated since the 1960s.[4] The perceived advantages of alkaline electrolytes (e.g., KOH solution) used in AFCs include the applications of nonprecious metal catalysts and increased fuel flexibility.[1,5] However, the use of liquid alkaline electrolytes has disadvantages such as maintaining containment of the electrolyte, component corrosion, and reaction with CO_2 to form insoluble carbonates that can block the electrodes, which must be scrubbed, necessitating the use of pumps and dramatically lowering system power density.[6] There is currently great interest in using AEMs in electrochemical devices, as the carbonate anion is mobile in these materials, the elimination of the liquid electrolyte increases system simplicity, and dramatically higher power densities can be achieved.[7,8]

Two limitations of AEMs must be overcome to enable practical applications: their inherently low conductivity (compared to proton exchange membranes) and the chemical stability of the organic cations that are susceptible to nucleophile attack by hydroxide in the operating device.[9,10] A large number of new chemistries have been proposed to overcome the two issues of needing high ionic conductivity and chemical stability. However, in order to design next generation AEMs we must correlate the cation chemistry with other membrane properties, e.g., anion and water transport, morphology, and water absorption, in order to better understand the performance of the AEM.[11−13] Simple quaternary ammonium cations have been studied extensively, as they provide good model systems and in certain membranes have been shown to have adequate stability, but they do not provide a route to the thousands of hours of transient operation required in many real devices.[14,15] Various second generation cations have been proposed for enhanced chemical stability including phosphonium,[16,17] pydridinium,[18] sulfonium,[19] imidazolium,[20,21] guanidinium,[22] and complex metal cations, e.g., (bis-terpyridine Ru).[23] Of particular interest are the imidazolium functionalized AEMs, which provide the following potential benefits: 1. Conjugated structures generated from

Received: March 20, 2014
Revised: June 23, 2014
Published: June 24, 2014

   dx.doi.org/10.1021/jp5027674 | J. Phys. Chem. C 2014, 118, 15136−15145

five heterocyclic rings help to delocalize positive charges, thus preventing nucleophilic attack by OH^- through Hofmann or S_N2 elimination.[24] 2. Imidazolium functionalized membranes may more favorably generate phase-separated morphologies.[25] 3. Imidazolium chemistry avoids the negative environmental effects of using trimethylamine. 4. The imidazolium cation is thermally more stable than the ammonium cation.[26]

To date studies on imidazolium functionalized AEMs have largely focused on conductivities, lifetime under alkaline conditions and the degradation mechanisms.[20,21,27−30] Zhang[30] and Guo[21] investigated AEMs with the same imidazolium cation but different polymer backbones (polysulfone, PSf-ImOH; poly(styrene-*co*-butyl methacrylate), PS-*co*-PBMA-Im). The chemical stabilities under alkaline conditions differ greatly. PSf-ImOH degrades in 3 M NaOH solution under 60 °C after 24 h, whereas PS-*co*-PBMA-Im is stable even after 120 h in 6 M NaOH under 80 °C. Thus, it has been proposed that imidazolium cation degradation is related to the membrane's backbone structure. The conductivity of PSf-ImOH is 16.1 mS/cm in water at 20 °C when IEC = 1.39 mequiv/g, while the conductivity for PS-*co*-PBMA-ImOH is 33.3 mS/cm at 30 °C with an IEC = 0.217 mequiv/g. Also, Deavin[20] made a comparison of benzyltrimethylammonium and 1-benzyl-3-methylimidazolium cationic groups with the same poly(ethylene-*co*-tetrafluoroethylene) (ETFE) backbone. The imidazolium functionalized ETFE has similar conductivity (the HCO_3^- conductivity increases from 16 mS/cm to 25 mS/cm from 30 to 60 °C, respectively, with an IEC = 1.8 mequiv/g) and lower chemical stability (1 M KOH solution under 60 °C) compared with the ammonium functionalized ETFE. More recently, Page[29] modified the imidazolium cation by attaching a methyl group on the carbon in the middle of two nitrogen (α-C) with the same AEM membrane. The conductivity was similar to that of the unmodified material (the HCO_3^- conductivity increases from 17.4 mS/cm to 27 mS/cm over the temperature range 30−60 °C), but the chemical stability did improve; however, it was still lower than that of the ammonium functionalized AEM. The degradation of the imidazolium cation under alkaline condition follows a ring-opening route by nucleophilic attack of OH^- groups on the α-C.[24,27] Therefore, the α-C position on the imidazolium cation is considered to be an effective location for modification. More research is still needed on α-C functional group replacement.[27,31]

To date, it is not known how a sterically bulky cation will affect the transport and morphological properties of an AEM. In this work we investigate a 1,4,5-trimethyl-2-(2,4,6-trimethoxyphenyl) imidazolium functionalized PPO (PPO-TMIM) (Figure 1). This sterically bulky cation was chosen because it was expected to have greater stability based on the contribution of the electron donating methyl groups as well as the α-C increased steric effect. OH^- has the highest intrinsic diffusion coefficient of the common anions used in AEMs. However, investigating the OH^- form of an AEM is often inconvenient, as ambient carbon dioxide (at publication time, 400 ppm) will react with the OH^- to form a mixture of CO_3^{2-} and HCO_3^- in the film. In this study, we investigated the films with Cl^- anions, as a surrogate for hydroxide as the films were supplied in the chloride form. We have recently shown that heavier halogen anions will enhance the transport of lighter halogen anions[32] and so we chose not to attempt to exchange the film for fluoride, which is more similar in size to hydroxide, as we did not want to risk studying a poorly characterized mixture of anions. However, we anticipate that the water-mediated transport of Cl^- in these films is still relevant to a general mechanism of anionic conductivity.

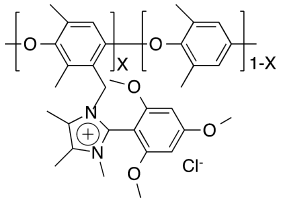

Figure 1. Structure of 1,4,5-trimethyl-2-(2,4,6-trimethoxyphenyl) imidazolium functionalized polyphenylene oxide.

In this paper, the chemical stability of the substituted imidazolium cation functionalized polymer under alkaline conditions was compared to the unsubstituted imidazolium functionalized PPO (PPO-IM). We also studied the morphology of the materials under different humidity conditions and further correlated this with transport behavior. The water diffusion was rationalized in terms of the conductivity, and the potential of the material as an AEM was evaluated.

2. EXPERIMENTAL SECTION

2.1. 1,4,5-Trimethyl-2-(2,4,6-trimethoxyphenyl) Imidazolium Functionalized PPO. 1,4,5-Trimethyl-2-(2,4,6-trimethoxyphenyl) imidazolium functionalized polyphenylene oxide (PPO-TMIM) was synthesized according to the literature.[33] The materials were in two imidazolium cation functionalization degrees, 33% and 46%, PPO-TMIM-0.33 and PPO-TMIM-0.46, with calculated IECs of 1.53 and 1.82 mequiv/g, respectively. An equivalent polymer with an unsubstituted imidazolium cation, PPO-IM, had a calculated IEC = 2.20 mequiv/g.

2.2. Ion Exchange Capacity. The ion exchange capacity (IEC) was measured by titrating the Cl^- form of the membrane using the Mohr method.[34] First, the Cl^- form membrane was soaked in 1 M aqueous sodium nitrate for 48 h under room temperature to release Cl^- ions. The mixed solution was titrated by standard $AgNO_3$ using K_2CrO_4 as a colorimetric indicator. The weight of the membrane was recorded after drying in a vacuum oven at 30 °C overnight. The IEC was calculated from eq 1. The quantity of $AgNO_3$ added is equal to the quantity of Cl^- after being ion exchanged by NO_3^-.

$$\mathrm{IEC} = \frac{V_{\mathrm{AgNO_3}} \times C_{\mathrm{AgNO_3}}}{m_{\mathrm{dry}}} \quad (1)$$

V_{AgNO_3} = volume of standard $AgNO_3$ solution consumed; C_{AgNO_3} = concentration of standard $AgNO_3$ solution; m_{dry} = mass of the dry membrane.

The theoretical IEC was calculated by using the number of fixed ionic groups in a repeating unit divided by the molecular weight of a repeating unit.[35]

2.3. Infrared Spectroscopy. Fourier transform infrared spectroscopy (FTIR) was recorded on a Nicolet Nexus 470 spectrometer with an attenuated total reflectance (ATR) accessory containing a diamond crystal. Spectra were obtained in the range 500−4000 cm^{-1}, with 256 scans and a resolution of 8 cm^{-1}.

dx.doi.org/10.1021/jp5027674 | J. Phys. Chem. C 2014, 118, 15136−15145

2.4. Thermogravimetric Analysis. Thermogravimetric analysis (TGA) was carried out using a SSC/5200 SII analyzer controlled by a TGDTA Measure thermal analysis station. Typically 5−8 mg samples were loaded into a platinum pan. Measurements were performed at a heating rate of 10 °C/min from 25 to 800 °C under a nitrogen atmosphere.

2.5. Dynamic Vapor Sorption. Water uptake of the membrane was tested by use of a SMS dynamic vapor sorption (DVS) instrument. The samples, after drying in a vacuum oven overnight, were loaded into a glass sample pan hanging from an ultrasensitive microbalance. The relative humidity was achieved by proportionally mixing dry gas (nitrogen) and a second water vapor stream controlled by a mass flow controller. The temperature of the experiments was set to 60 °C for the different humidity cycles. Samples were first kept at 0% RH for 8 h; then the humidity was increased in the sequence: 20%, 40%, 60%, 80%, 95%, and then deceased to 0% with the same humidity steps. Each humidity condition was held for 2 h and the cycle was run twice. The equilibrium mass at the end of each step was used to calculate the water uptake from the isotherm of mass versus relative humidity. The water uptake was calculated according to eq 2.

$$\mathrm{WU}(\%) = 100\% \times \frac{m_{\mathrm{RH}} - m_{\mathrm{dry}}}{m_{\mathrm{dry}}} \tag{2}$$

m_{RH} = mass of the sample under different relative humidity; m_{dry} = mass of the sample under 0% RH.

The hydration number, λ, representing the number of water molecules per cationic group was calculated from eq 3.

$$\lambda = \frac{\mathrm{WU}}{M_{\mathrm{H_2O}} \times \mathrm{IEC}} \tag{3}$$

$M_{\mathrm{H_2O}}$ = molar mass of water.

2.6. Small Angle X-ray Scattering. Small angle X-ray scattering (SAXS) was performed at the Advanced Photon Source (APS), Argonne National Laboratory, on beamline 12ID-B. The beam wavelength was λ = 0.886 Å, with an exposure time of 1 s, and an energy of E = 14 keV. Two-dimensional scattering patterns were collected simultaneously with a 25 × 29 cm^2 area Pilatus 2 M detector. The one-dimensional intensity versus q plot was azimuth averaged from the 2D scattering pattern for the SAXS in the range of 0.003 $\mathrm{Å}^{-1} < q < 0.5\ \mathrm{Å}^{-1}$, where $q = 4\pi\lambda^{-1}\sin(\theta)$. The data were converted to a differential cross section.

A custom-made four-sample oven was used to control both humidity and temperature.[36] The oven had Kapton windows. One slot was left blank and used as the background, while the other three sample slots contained membrane samples. Experimental data was measured from 0% RH to 95% RH as well as for membranes that had been soaked in water. For each humidity step, 20−40 min were used to equilibrate after changing the humidity. The soaked sample was immersed in DI water for 24 h before measurements.

2.7. Microscopy. Atomic force microscopy (AFM) images were taken in tapping mode using a Bruker Nanoscope III instrument with high-aspect-ratio 225 μm cantilever tips (Nanoworld NCLR). Analysis was performed using Nanoscope 5.30r1 software. The dry sample was evacuated in a vacuum oven overnight at room temperature. The wet sample was treated in DI water for 24 h, and then imaged immediately under ambient conditions.

Micrometer-scale morphologies of the membranes were acquired using a Thermo Fisher Nicolet iN10 microscope. The image was collected in transmission mode on the membrane soaked in DI water for 24 h under room temperature.

2.8. Pulsed-Field Gradient Nuclear Magnetic Resonance. ^{1}H self-diffusion coefficients were obtained by use of pulsed-field gradient nuclear magnetic resonance (PFG NMR) on an AVANCEIII NMR spectrometer with a 5 mm Bruker single-axis DIFF60L Z-diffusion probe. The pulsed field gradient at 26 °C was varied from 0 to 128 G/cm over 16 randomized steps. The NMR frequency was 400 MHz and data was analyzed with Bruker TopSpin software. The decay of signal intensity could be expressed with the Stejskal-Tanner equation[37,38] given in eq 4 when the transport was only related within the z direction.

$$\frac{A(g)}{A(0)} = \exp(-\gamma^2 g^2 \delta^2 t_{\mathrm{d}} D) \tag{4}$$

$A(g)$ = echo amplitude; $A(0)$ = amplitude of the spin−echo signal in the absence of pulsed field gradient; γ = gyromagnetic ration; g = amplitude of field gradient pulse; δ = duration of the field gradient pulse; t_{d} = diffusion time ($t_{\mathrm{d}} = \Delta - \delta/3$, where Δ is the time interval between the gradient pulses); D = self-diffusion coefficient.

The membrane sample was wound into a completely sealed 5 mm tube above a salt solution at the bottom providing 80% RH. The experiment was performed at 80% RH from 26 to 45 °C.

2.9. Electrochemical Impedance Spectroscopy. In-plane anionic conductivity was calculated by use of electrochemical impedance spectroscopy (EIS) based on the measurement of the ionic resistance.[39] The Randle's equivalent electrical circuit was used to fit the measured Nyquist Plot. The intercept at the lower frequency was used to determine the total ionic resistance. The frequency range was from 0.4 to 10^5 Hz with a fixed voltage magnitude of 10 mV. The membrane was mounted in a four-electrode cell connected to a BioLogic VMP3 multichannel potentiostat. The conductivity was calculated from the equation shown below.

$$\sigma = \frac{l}{RS} \tag{5}$$

σ = conductivity, (S/cm); R = resistance, (Ω); S = cross section area of the membrane, (cm^2); l = length of the membrane tested between two electrodes, (cm).

An environmental chamber (Test Equity) was used to control both humidity and temperature during the experiment. The measurements were performed from 50 to 90 °C under 95% RH. Each testing condition ran for 16 loops with the first 8 loops for membrane equilibration under the conditions and the last 8 loops for data analysis.

2.10. Degradation Studies. Chemical stability measurements were performed by treating PPO-TMIM and PPO-IM in 1 M sodium hydroxide solution at 80 °C The degradation of cationic groups were determined in terms of the IEC based on the titration of Cl^- form membranes as described above in section 2.2.

3. RESULTS AND DISCUSSION

3.1. Structure Verification. The polymer structure was first validated by NMR and was shown to match the literature spectra.[33] The FTIR spectra (Figure 2) of polyphenylene oxide,

dx.doi.org/10.1021/jp5027674 | J. Phys. Chem. C 2014, 118, 15136−15145

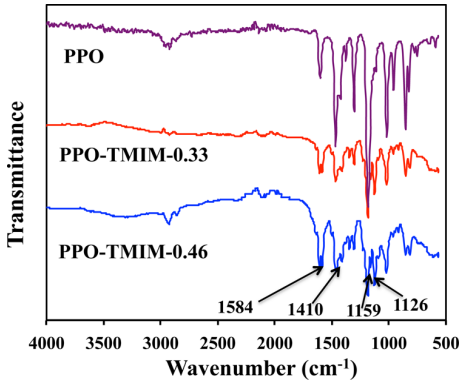

Figure 2. FTIR spectra of polyphenylene oxide, top, and the 1,4,5-trimethyl-2-(2,4,6-trimethoxy phenyl) imidazolium functionalized polyphenylene oxides, middle and bottom.

PPO-TMIM-0.33 and PPO-TMIM-0.46, are compared. Both PPO-TMIM-0.33 and PPO-TMIM-0.46 display additional peaks when compared to the base PPO material (Figure 2, top trace) at 1584, 1410, 1159, and 1126 cm^{-1}. The 1584 and 1126 cm^{-1} peaks are ascribed to C═N and C—N stretching, respectively, while the peaks at 1410 and 1159 cm^{-1} are assigned to the imidazole ring asymmetric stretch and C—H vibrations.[20,40]

3.2. Chemical and Thermal Stability Studies. We compare the chemical stability of the modified and unsubstituted imidazolium functionalized PPO polymers in Figure 3.

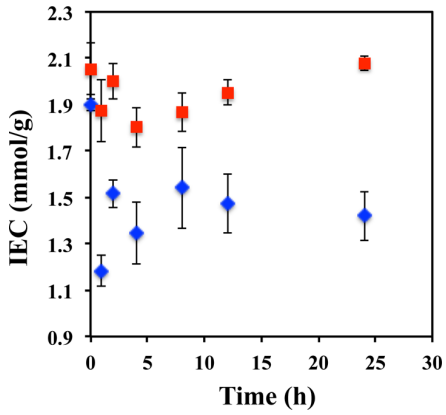

Figure 3. IEC of 1,4,5-trimethyl-2-(2,4,6-trimethoxyphenyl) imidazolium functionalized polyphenylene oxide (■ PPO-TMIM-0.46) and unsubstituted imidazolium functionalized poly phenylene oxide (◆ PPO-IM) during the alkaline stability test at 80 °C in 1 M KOH.

Initial measured IECs of PPO-TMIM-0.46 and PPO-IM were 2.0 and 1.9 mequiv/g. The IEC of substituted PPO-TMIM polymer decreases more slowly initially than that of PPO-IM as shown in Figure 3, and both showed a higher IEC at the end than the minimum values recorded. After 24 h of hydroxide treatment at 80 °C, the IEC of PPO-TMIM was unchanged from the initial value, whereas the IEC of PPO-IM had decreased by 25%. It is possible that the minimum value of the IEC is the true value for the degraded film and that the gradual recovery of the IEC is due to entrapped salt that cannot be easily washed from the film; nevertheless, the PPO-IM polymer is clearly quite unstable under the test conditions. Other AEMs recently reported also display this degradation phenomenon.[41]

The enhanced bacisity of the modified imidazolium due to the electron donating methyl and trimethoxyphenyl groups as well as the static effect from the large trimethoxyphenyl group efficiently prevent nucleophilic OH^- attack on the α-C position of the imidazole ring as compared to the unsubstituted imdazolium cation. This improved long-term stability of PPO-TMIM was also demonstrated by Wang[33] under the same degradation conditions.

The thermal gravimetric analysis curves and the derivative of the thermal gravimetric curves for PPO-TMIM-0.46 and PPO-TMIM-0.33 are shown in Figure 4. The TGA measurements

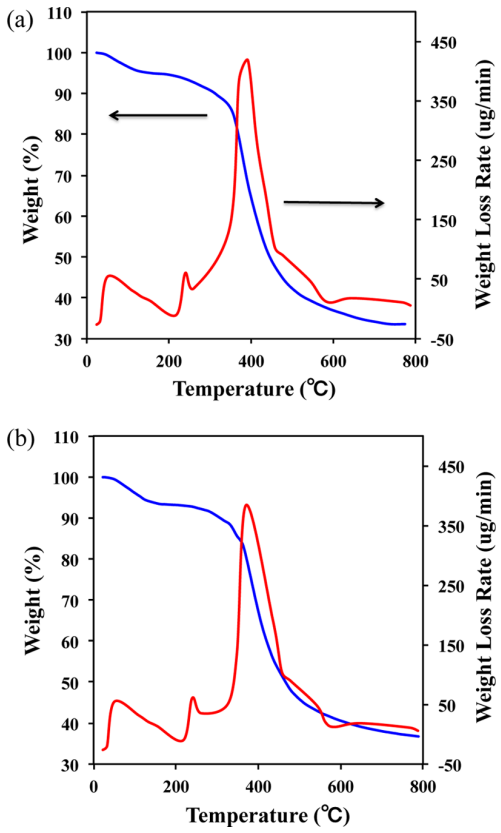

Figure 4. Thermal gravimetric analysis curves and derivative thermal gravimetric curves of 1,4,5-trimethyl-2-(2,4,6-trimethoxyphenyl) imidazolium functionalized polyphenylene oxide: (a) PPO-TMIM-0.33, (b) PPO-TMIM-0.46.

have three weight loss regions corresponding to the highest weight loss rates at ca. 50 °C, 240 °C for both polymers and 392 or 370 °C for PPO-TMIM-0.33 or PPO-TMIM-0.46, respectively. The first mass loss stage corresponds to water losses of 5% (PPO-TMIM-0.33) and 6% (PPO-TMIM-0.46). The second weight loss corresponds to the onset of decomposition temperature at 217 °C and is attributed to the nucleophilic attack of chloride anions through a S_N2 reaction to the 1,4,5-trimethyl-2-(2,4,6-trimethoxyphenyl) imidazolium cation.[26,42] This onset decomposition temperature is higher than for quaternary ammonium or the unmodified imidazolium cation.[30] The third region of mass loss results from the decomposition of the PPO aromatic chains.[25] Both the chemical and thermal stabilities of this AEM, PPO-TMIM, confirm a promising application in AFCs.

dx.doi.org/10.1021/jp5027674 | J. Phys. Chem. C 2014, 118, 15136−15145

3.3. Morphological Studies. The DVS data, discussed below, reveals that water sorption of the PPO-TMIM-0.46 polymer is 5% higher in absolute value and 30% higher in relative value than the PPO-TMIM-0.33 polymer at 95% RH. This leads to observable differences in the membrane morphologies. The effects of water on the morphology are exhibited in the AFM phase-contrast images in Figure 5. Figure 5a shows that the dry membrane is homogeneous. After the absorption of water, the membrane clearly shows the formation of clusters, which are likely due to the aggregation of hydrophilic and hydrophobic groups as shown in Figure 5b,c. Care must be taken in the interpretation of the phase contrast in these images. Previous reports on related AEMs have suggested that regions of lower phase (dark regions) correspond to hydrophilic domains, while regions with higher phase (bright regions) correspond to hydrophobic domains.[25,43] However, the slope of any morphological features contributes directly to the phase, due to the finite response time of the instrument feedback loop.[44] Thus, the dark regions at the cluster boundaries have been significantly influenced by the abrupt changes in morphology observed in the height images (Supporting Information, Figure 1). The data is therefore used in conjunction with the SAXS data described below to confirm the cluster size.

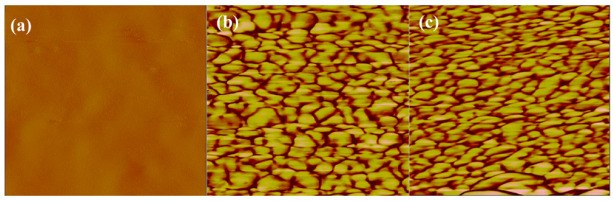

Figure 5. AFM tapping mode phase images of 1,4,5-trimethyl-2-(2,4,6-trimethoxyphenyl) imidazolium functionalized polyphenylene oxide: PPO-TMIM-0.46, (a) dry, phase scale = 5°; (b) wet, phase scale = 20°. PPO-TMIM-0.33, (c) wet, phase scale = 20°. Scan boxes are 500 nm × 500 nm.

The root mean square (RMS) roughness of wet PPO-TMIM-0.46 is 3.53 nm while that of wet PPO-TMIM-0.33 is 2.21 nm, indicating that the clusters are taller in PPO-TMIM-0.46. Both wet films are significantly rougher than the dry PPO-TMIM-0.46 film, which has an RMS roughness of 1.37 nm. By using ImageJ to analyze the bright domain sizes (Table 1), it was found that PPO-TMIM-0.46 embraces a more even distribution with 30 (SD, 10) nm average Feret diameter compared to a smaller 25 (SD, 13) nm average Feret diameter of PPO-TMIM-0.33. Thus, the wet PPO-TMIM-0.46 material forms larger volume clusters than the wet PPO-TMIM-0.33 material.

Table 1. ImageJ Analysis of Feret Diameters, SD of Size Distributions, and RMS Roughness of Wet 1,4,5-Trimethyl-2-(2,4,6-Trimethoxyphenyl) Imidazolium Functionalized Polyphenylene Oxide Films

sample designation	average of Feret diameters (nm) (bright domain)	standard deviations (SD) of size distribution (nm) (bright domain)	RMS roughness
PPO-TMIM-0.33	25	13	2.21
PPO-TMIM-0.46	30	10	3.53

SAXS was used as a method for detecting the average phase morphology of the bulk materials.[45,46] Based on monitoring bulk morphology variations along with humidity from SAXS, it is noticed that there is no long-range ordered configuration (e.g., lamellae) exhibited owing to the random copolymer structure, unlike a typical block copolymer which embraces long regular alternating junctions that probably enable a highly ordered configuration from the hydrophobic and hydrophilic domain arrangement.[12,47] However, some ionomer patterns designated from the q range around 0.2 Å^{-1} are exhibited. The large full width at half-maximum (fwhm) of the ionomer peaks again indicates a weak long-range order of the structure. This ionomer pattern becomes more irregular when the humidity increases from 0% RH to 95% RH but is rearranged into a more ordered configuration again by soaking the membrane in water. The new ionomer peak with an improved scattering intensity moves toward a smaller q range after soaking the membrane in water because of the expanded ionomer domain sizes. The differences between PPO-TMIM-0.33 and PPO-TMIM-0.46 are illustrated by the scattering slope variation at the q range of 0.003−0.02 Å^{-1} from dry to wet condition (Figure 6). For the low IEC sample, the Porod slope increases from 3.1 to 3.6 when the humidity is increased from 0% to 95% RH, indicating an increase in symmetry; while the observation for the high IEC sample was contrary, with a scattering slope decrease from 3.6 to 3.0 as the particle configuration loses its symmetry. Moreover, comparing SAXS patterns between PPO-TMIM-0.46 and PPO-TMIM-0.33 under high humidity conditions, a

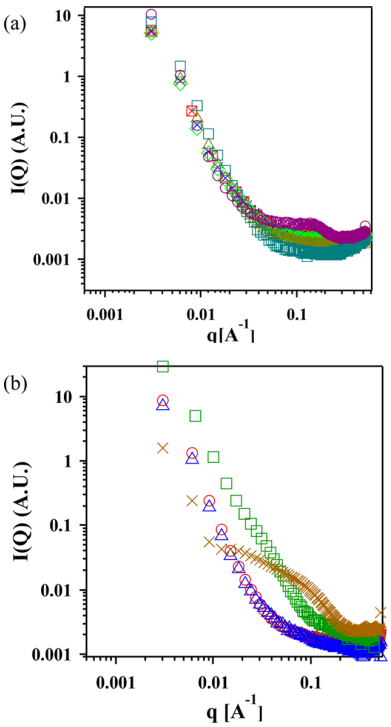

Figure 6. SAXS patterns of 1,4,5-trimethyl-2-(2,4,6-trimethoxyphenyl) imidazolium functionalized polyphenylene oxide: (a) PPO-TMIM-0.33 and (b) PPO-TMIM-0.46 (key: (a) boxed ×, PPO-TMIM-0.33 dry, × PPO-TMIM-0.33 25% RH, ◇ PPO-TMIM-0.33 50% RH, △ PPO-TMIM-0.33 75% RH, □ PPO-TMIM-0.33 95% RH, ○ PPO-TMIM-0.33 soaked; (b) ○ PPO-TMIM-0.46 dry, △ PPO-TMIM-0.46 25% RH, □ PPO-TMIM-0.46 95% RH, × PPO-TMIM-0.46 soaked).

dx.doi.org/10.1021/jp5027674 | J. Phys. Chem. C 2014, 118, 15136−15145

new shoulder can be seen with the d spacing in the range of 10−32 nm, which corresponds to the uniformly distributed clusters of PPO-TMIM-0.46 observed in the AFM (Figure 5b). Both the shoulder and ionomer domain length scales from the SAXS are consistent with the bright and dark dimensions shown in AFM as quantified by ImageJ.

3.4. Water Sorption. The water sorption values for PPO-TMIM-0.33 and PPO-TMIM-0.46 are 17% and 22% (Figure 7), respectively, corresponding to λ of 6 and 7 under 95% RH

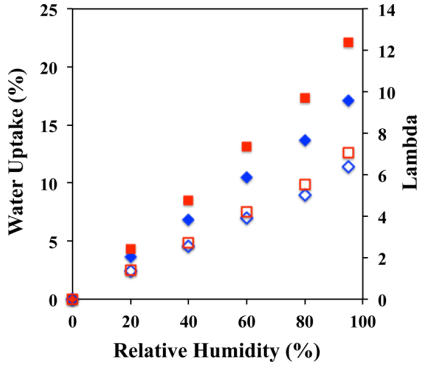

Figure 7. Water uptake values and hydration numbers of 1,4,5-trimethyl-2-(2,4,6-trimethoxyphenyl) imidazolium functionalized polyphenylene oxide. (water uptakes: ■ PPO-TMIM-0.46, ◆ PPO-TMIM-0.33; hydration numbers: □ PPO-TMIM-0.46, ◇ PPO-TMIM-0.33).

at 60 °C. λ values for PPO-TMIM-0.33 and PPO-TMIM-0.46 are almost the same at 40% RH and only 10% different at 95% RH. The water uptake of both PPO-TMIM-0.33 and PPO-TMIM-0.46 at ambient humidity (23% RH) are slightly lower than the TGA weight losses (PPO-TMIM-0.33 and PPO-TMIM-0.46 weight losses are 5% and 6%) from bound water. The reason is due to the small amount of bound water left when drying the sample in the DVS at low temperature for the purpose of preventing sample damage.

3.5. Water Self-Diffusion Inhibited in Polymer. The PFG NMR technique was used to add further insight into the overall transport properties and relate this to the membrane morphology. In restricted diffusion, the time-dependent region engages interactions of water molecules with membrane walls, while in the time-independent region all the diffusion is fully hindered inside the membrane walls and achieves D_∞.[48] Therefore, diffusion at different time intervals between gradient pulses are determined by the complexity of the membrane and it in turn reflects the anisotropy of the membrane.

Figure 8 shows the diffusion coefficient as a function of the evolution time in the PFG NMR experiment. Diffusion coefficients of both PPO-TMIM-0.33 and PPO-TMIM-0.46 decline along with the diffusion time indicating a restricted diffusion. The nanoscale morphology shown in AFM and SAXS gives rise to a weak diffusion dependence (slopes are -2×10^{-6} for PPO-TMIM-0.33, -5×10^{-6} cm^2/s^2 for PPO-TMIM-0.46) as a result of the tortuosity of the membrane. D_∞ of PPO-TMIM-0.33 and PPO-TMIM-0.46 are 1.3×10^{-6} cm^2/s and 1.0×10^{-6} cm^2/s, respectively, when full geometrical restriction is achieved.

The Mitra equation[48,49] shown in eq 6 is used to further analyze the influence of the membrane morphology on the diffusion properties. This provides insights into phase complexities such as the overall size under which water molecules move freely or the tortuous ion conducting pathways in the membrane. Furthermore, the diffusion coefficient D_0, when only Brownian motion occurs, can be obtained from extrapolation of D to $t_d = 0$.

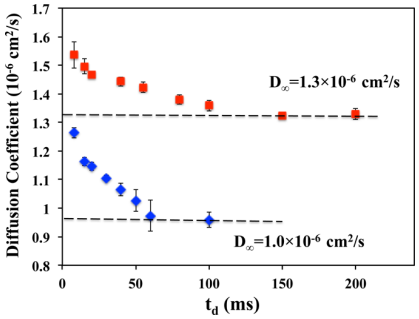

Figure 8. Water self-diffusion coefficients of 1,4,5-trimethyl-2-(2,4,6-trimethoxyphenyl) imidazolium functionalized polyphenylene oxide versus diffusion time. The measurement was taken under 80% RH at 26 °C (■ PPO-TMIM-0.33, ◆ PPO-TMIM-0.46).

$$D = D_0\left[1 - \frac{4}{9\sqrt{\pi}} \cdot \frac{S}{V} \cdot \sqrt{D_0 \cdot t_d}\right] \quad (6)$$

where S/V is the surface-to-volume ratio of the porous material. From Figure 9, D_0 of PPO-TMIM-0.46 and PPO-TMIM-0.33

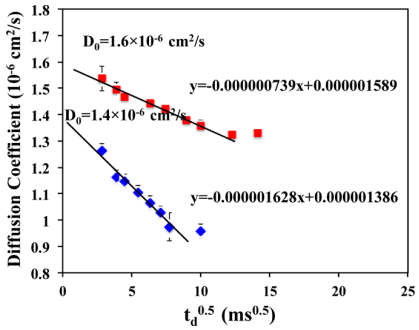

Figure 9. Water self-diffusion coefficients of 1,4,5-trimethyl-2-(2,4,6-trimethoxyphenyl) imidazolium functionalized polyphenylene oxide versus the square root of the diffusion time. The measurement was taken under 80% RH at 26 °C (■ PPO-TMIM-0.33, ◆ PPO-TMIM-0.46).

calculated according to eq 6 are 1.4×10^{-6} cm^2/s and 1.6×10^{-6} cm^2/s, respectively, which are lower than the bulk water diffusion coefficient 2.3×10^{-5} cm^2/s at 25 °C.[11] Our nanometer-scale clusters observed in SAXS and AFM make water transport in the hydrophilic domains at $t_d = 0$ much slower than the bulk water transport, which is due to the effect from the hydrated polymeric environment inside the channels.[50]

S/V in the Mitra equation can be obtained from the slope in Figure 9. R_c, the reciprocal of S/V, is a critical parameter that designates the structure length scale within which intradomain transport is dominant.[51,52] From Table 2, we observed that R_c values of both PPO-TMIM-0.46 and PPO-TMIM-0.33 are much larger than cluster sizes shown in AFM and SAXS. By comparing R_c values between PPO-TMIM-0.46 and PPO-TMIM-0.33, it is noticed that even though PPO-TMIM-0.33 embraces a lower water uptake, R_c of PPO-TMIM-0.33 is still

dx.doi.org/10.1021/jp5027674 | J. Phys. Chem. C 2014, 118, 15136−15145

Table 2. Surface/Volume Ratio, R_c, and Tortuosity for 1,4,5-Trimethyl-2-(2,4,6-Trimethoxyphenyl) Imidazolium Functionalized Polyphenylene Oxides

sample designation	S/V (μm^{-1})	R_c (μm)	tortuosity (α)
PPO-TMIM-0.33	0.15	6.7	1.18
PPO-TMIM-0.46	0.39	2.6	1.47

larger than that of PPO-TMIM-0.46. The tortuosity of the membrane is calculated from eq 7.[53]

$$D_\infty = D_0\alpha^{-1} \tag{7}$$

where α is the tortuosity. From Table 2, the tortuosity of PPO-TMIM-0.33, calculated by eq 7, is smaller than that of PPO-TMIM-0.46. Smaller tortuosity designates a less morphological barrier for transport. The smaller cluster sizes of PPO-TMIM-0.33 observed in AFM give rise to more junctions of dark domains so that promote transport pathway connections. Hence, PPO-TMIM-0.33, which embraces a smaller tortuosity, makes itself into a larger critical length scale and possesses a weaker dependence on diffusion time, even though it has a lower water uptake.

The diffusion length, which relates the diffusion coefficient, D, to the diffusion time, t_d, is calculated according to eq 8[54]

$$\langle a^2\rangle^{1/2} = \sqrt{2Dt_d} \tag{8}$$

where $\langle a^2\rangle^{1/2}$ is the diffusion length. By plotting the diffusion coefficient versus diffusion length (Figure 10), the fully

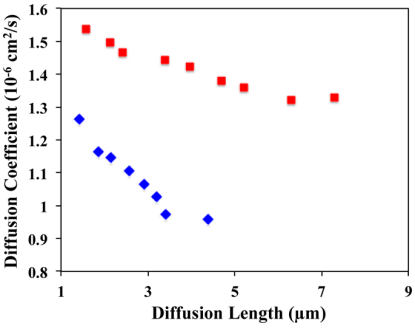

Figure 10. Water self-diffusion coefficients of 1,4,5-trimethyl-2-(2,4,6-trimethoxyphenyl) imidazolium functionalized polyphenylene oxide versus diffusion length (■ PPO-TMIM-0.33, ◆ PPO-TMIM-0.46).

restricted domain size is observed when the diffusion coefficient levels off. We noticed that fully restricted length scales of PPO-TMIM-0.33 and PPO-TMIM-0.46 are 6.3 and 3.4 μm, respectively, which are in line with the R_c values, 6.7 μm of PPO-TMIM-0.33 and 2.6 μm of PPO-TMIM-0.46, obtained from Mitra equation. Thus, the length scale of intradomain transport of water molecules extends into the micrometer scale.

We used visible microscopy to verify that the membrane had morphological features on the micrometer scale (Figure 11). Both PPO-TMIM-0.33 and PPO-TMIM-0.46 display small circular patterns ca. 5 μm and larger black dots at ca. 10−15 μm that might comprise smaller length-scale structures. These micrometer order of magnitude lengths and nanoscale domains shown in SAXS and AFM compose a hierarchical structure. Thus, the interconnected hydrophilic channels facilitate water-molecule transport into a larger length scale (on the

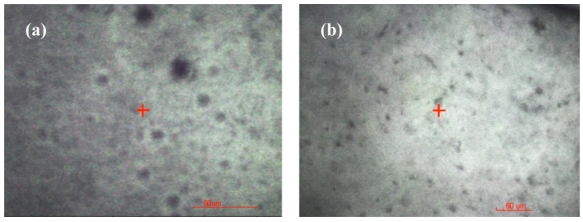

Figure 11. Visible microscope images of 1,4,5-trimethyl-2-(2,4,6-trimethoxyphenyl) imidazolium functionalized polyphenylene oxide: (a) PPO-TMIM-0.33, (b) PPO-TMIM-0.46.

micrometer scale, Figure 10) beyond the dimensions observed in SAXS and AFM (on the nanometer scale).

The self-diffusion coefficients of water for the two polymers as a function of temperature are shown in Figure 12. Both the

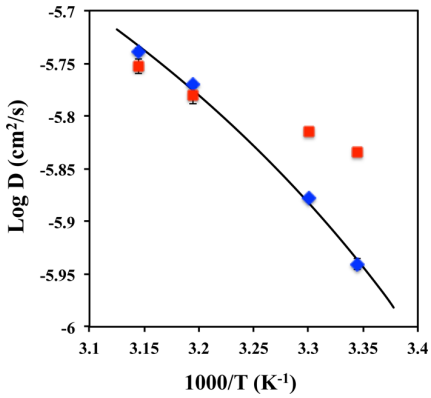

Figure 12. Arrhenius plot of water self-diffusion coefficients under 80% RH. The measurements were performed at Δ = 20 ms (■ PPO-TMIM-0.33, ◆ PPO-TMIM-0.46).

PPO-TMIM-0.46 and PPO-TMIM-0.33 diffusion coefficients increase along with temperature. The low IEC sample shows a linear relationship with an E_a of 7 ± 0.3 kJ/mol, while the high IEC sample displays a nonlinear, convex, super-Arrhenius behavior. The membrane with higher water uptake, PPO-TMIM-0.46, shows a larger diffusion coefficient at a higher temperature (above 40 °C), which is in line with the conductivity result in Figure 13, even though the water diffusion does not necessarily exhibit a linear relation or proportionality to conductivity.[11]

3.6. Conductivity. The Cl^- form conductivities of PPO-TMIM-0.46 and PPO-TMIM-0.33, under 95% RH at 90 °C, are 23 mS/cm and 16 mS/cm, respectively (Figure 13), and are comparable with other imidazolium functionalized AEMs.[20,21,29,30] The Arrhenius plot of PPO-TMIM-0.33 exhibits a linear behavior from 50 to 90 °C. The E_a of PPO-TMIM-0.33 is 15 ± 2 kJ/mol, indicating a water mediated vehicle mechanism, and is slightly lower than other imidazolium AEMs.[21,55] The Nernst−Einstein equation[56] shown below is used to distinguish the conducting mechanism through the comparison of water diffusion coefficients from PFG NMR with calculated Cl^- diffusion coefficients.

$$D = RT\frac{\kappa}{cz^2F^2} \tag{9}$$

where D is the diffusion coefficient, κ is the conductivity, c is the concentration of anionic groups in the membrane, z is the

dx.doi.org/10.1021/jp5027674 | J. Phys. Chem. C 2014, 118, 15136−15145

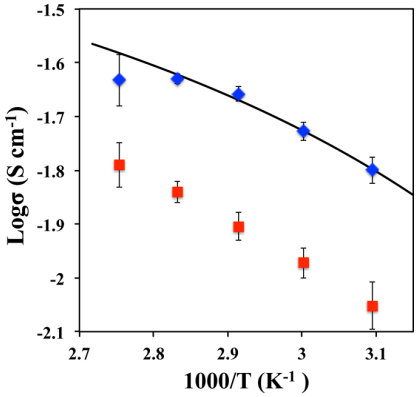

Figure 13. Cl^- form conductivities of 1,4,5-trimethyl-2-(2,4,6-trimethoxyphenyl) imidazolium functionalized polyphenylene oxide under 95% RH (■ PPO-TMIM-0.33, ◆ PPO-TMIM-0.46).

ionic charge, F is the Faraday constant, R is the gas constant, and T is the temperature. The Cl^- diffusion coefficient of PPO-TMIM-0.33, calculated based on eq 9, is 1.55×10^{-6} cm^2/s, which is smaller than the water diffusion coefficient, 1.77×10^{-6} cm^2/s, under 45 °C and 80% RH. Therefore, the Cl^- diffuses more slowly than water via the vehicle mechanism, because the solvated Cl^- is larger than the water molecules. Appling the same calculation on PPO-TMIM-0.46, the Cl^- diffusion coefficient is 1.56×10^{-6} cm^2/s, which is also smaller than the water diffusion coefficient, 1.82×10^{-6} cm^2/s. However, the conductivity data for the PPO-TMIM-0.46 membrane, exhibits a super Arrhenius behavior similar to that of the water diffusion. We can fit both the ionic conductivity and water diffusion data for the high IEC polymer to the Vogel–Tammann–Fulcher (VTF) equation shown below.[57−60]

$$\sigma(T) = \sigma_0 \exp\left(-\frac{b}{T - T_0}\right)$$
$$D(\mathrm{T}) = D_0 \exp\left(-\frac{b}{T - T_0}\right) \quad (10)$$

where σ_0 and D_0 are the conductivity and diffusion coefficients at infinite temperature, b is a constant related to the entropic barrier to free volume creation, T_0 is the temperature at which the mobility of ions and the conductivity drop to zero. Based on the three-parameter fit by using of Mathematica (Table 3),

Table 3. Parameters of VTF Regression of PPO-TMIM-0.46 on Both Conductivity and Diffusion Coefficients versus Temperatures

VTF regression	σ_0 (S/cm), D_0 (cm^2/s)	b (K)	T_0 (K)
conductivity	0.075	132	238
diffusion coefficient	7.1×10^{-6}	100	244

T_0 from the PFG NMR water diffusion coefficient and the EIS Cl^- conductivity data fits are similar, ca. 240 K, which is nominally considered 50 K lower than the T_g of the material.[61,62] We assign this to the T_b, 290 K, of the hydrophilic phase. The b value obtained is higher, 132 K, for ionic conductivity of Cl^- than for water diffusion from PFG-NMR, 100 K, indicating that Cl^- is energetically less mobile than H_2O in the channel. The maximum conductivity of Cl^- is calculated to be 0.075 S/cm and of water diffusion 7.1×10^{-6} cm^2/s which is an order of magnitude smaller than for free water at room temperature, 2.3×10^{-5} cm^2/s, again indicative of the highly hindered transport in these polymers.

4. CONCLUSION

In this study, a novel 1,4,5-trimethyl-2-(2,4,6-trimethoxyphenyl) imidazolium functionalized PPO polymer was studied. The increased electron donating and steric bulk of the cation enhanced the AEM durability compared to the unsubstituted imidazolium functionalized PPO, over 24 h without any degradation in 1 M KOH solution at 80 °C. In addition, the PPO-TMIM polymers have good thermal stabilities. From AFM, the membrane exhibited a homogeneous morphology under dry conditions, compared to clusters formation in the humidified films. The average Feret diameters of clusters of PPO-TMIM-0.33 and PPO-TMIM-0.46 were 25 and 30 nm, respectively, analyzed by ImageJ. The domain sizes in AFM corresponded to the d spacing (3 nm and 10−32 nm) displayed in the SAXS patterns. Transport studies showed a high dependency on the morphology of the membrane. Free water diffusion coefficients in the polymers were ca. 1.5×10^{-6} cm^2/s, that is, smaller than the diffusion in bulk water. Long-range diffusion coefficients D_∞ were ca. 1.0×10^{-6} cm^2/s due to restrictions on the micrometer scale as seen in the visible micrographs.

The high IEC PPO-TMIM-0.46 displayed a high conductivity of 23 mS/cm in Cl^- form at 95% RH and 90 °C. Interestingly, the low IEC polymer exhibited Arrhenius behavior following a vehicle mechanism in its transport properties, whereas the high IEC polymer showed super Arrenhius behavior, which could be fit to a VTF model as the ion transport was facilitated by the movement of the cationic side chains in the hydrophilic phase. As the content of the large cation is increased in the hydrophilic channels, the ions clearly do not move in a fully dissociated manner uninfluenced by the cation chemistry.

■ ASSOCIATED CONTENT

Ⓢ Supporting Information

Further analysis of the relation between the AFM height and phase images. This material is available free of charge via the Internet at http://pubs.acs.org

■ AUTHOR INFORMATION

Corresponding Author

*Phone: (303) 384-2082. Fax: (303) 273-3730. E-mail: aherring@mines.edu.

Notes

The authors declare no competing financial interest.

■ ACKNOWLEDGMENTS

The authors thank the Army Research Office for support of this research under the MURI grant number #W911NF-10-1-0520. The Advanced Photon Source operated for the U.S. Department of Energy (DOE) Office of Science by Argonne National Laboratory was supported by the U.S. DOE under Contract No. DE-AC02-06CH11357. We also thank James L. Horan and Tara P. Pandey for help with visible microscopy measurement.

■ REFERENCES

(1) Spendelow, J. S.; Wieckowski, A. Electrocatalysis of Oxygen Reduction and Small Alcohol Oxidation in Alkaline Media. *Phys. Chem. Chem. Phys.* **2007**, *9*, 2654−2675.

(2) Varcoe, J. R.; Slade, R. C. T.; Lam How Yee, E. An Alkaline Polymer Electrochemical Interface: A Breakthrough in Application of Alkaline Anion-Exchange Membranes in Fuel Cells. *Chem. Commun.* **2006**, 1428−1429.
(3) Hickner, M. A.; Herring, A. M.; Coughlin, E. B. Anion Exchange Membranes: Current Status and Moving Forward. *J. Polym. Sci., Part B* **2013**, *51*, 1727−1735.
(4) Merle, G.; Wessling, M.; Nijmeijer, K. Anion Exchange Membranes for Alkaline Fuel Cells: A Review. *J. Membr. Sci.* **2011**, *377*, 1−35.
(5) McLean, G. F.; Niet, T.; Prince-Richard, S.; Djilali, N. An Assessment of Alkaline Fuel Cell Technology. *Int. J. Hydrogen Energy* **2002**, *27*, 507−526.
(6) Varcoe, J. R.; P, S. D.; Slade, R. C. T. Alkaline Anion-Exchange Membranes for Low-Temperature Fuel Cell Application. *Handbook of Fuel Cells* **2009**, *5*, 322−323.
(7) Cifrain, M.; Kordesch, K. V. Advances, Aging Mechanism and Lifetime in Afcs with Circulating Electrolytes. *J. Power Sources* **2004**, *127*, 234−242.
(8) Varcoe, J. R.; Slade, R. C. T. Prospects for Alkaline Anion-Exchange Membranes in Low Temperature Fuel Cells. *Fuel Cells* **2005**, *5*, 187−200.
(9) Neagu, V.; Bunia, I.; Plesca, I. Ionic Polymers - Vi. Chemical Stability of Strong Base Anion Exchangers in Aggressive Media. *Polym. Degrad. Stab.* **2000**, *70*, 463−468.
(10) Zagorodni, A. A.; Kotova, D. L.; Selemenev, V. F. Infrared Spectroscopy of Ion Exchange Resins: Chemical Deterioration of the Resins. *React. Funct. Polym.* **2002**, *53*, 157−171.
(11) Hibbs, M. R.; Hickner, M. A.; Alam, T. M.; McIntyre, S. K.; Fujimoto, C. H.; Cornelius, C. J. Transport Properties of Hydroxide and Proton Conducting Membranes. *Chem. Mater.* **2008**, *20*, 2566−2573.
(12) Simone, P. M.; Lodge, T. P. Phase Behavior and Ionic Conductivity of Concentrated Solutions of Polystyrene-Poly(Ethylene Oxide) Diblock Copolymers in an Ionic Liquid. *ACS Appl. Mater. Interfaces* **2009**, *1*, 2812−2820.
(13) Weber, R. L.; Ye, Y. S.; Schmitt, A. L.; Banik, S. M.; Elabd, Y. A.; Mahanthappa, M. K. Effect of Nanoscale Morphology on the Conductivity of Polymerized Ionic Liquid Block Copolymers. *Macromolecules* **2011**, *44*, 5727−5735.
(14) Edson, J. B.; Macomber, C. S.; Pivovar, B. S.; Boncella, J. M. Hydroxide Based Decomposition Pathways of Alkyltrimethylammonium Cations. *J. Membr. Sci.* **2012**, *399*, 49−59.
(15) Sata, T.; Tsujimoto, M.; Yamaguchi, T.; Matsusaki, K. Change of Anion Exchange Membranes in an Aqueous Sodium Hydroxide Solution at High Temperature. *J. Membr. Sci.* **1996**, *112*, 161−170.
(16) Gu, S.; Cai, R.; Luo, T.; Chen, Z. W.; Sun, M. W.; Liu, Y.; He, G. H.; Yan, Y. S. A Soluble and Highly Conductive Ionomer for High-Performance Hydroxide Exchange Membrane Fuel Cells. *Angew. Chem., Int. Ed.* **2009**, *48*, 6499−6502.
(17) Noonan, K. J. T.; Hugar, K. M.; Kostalik, H. A.; Lobkovsky, E. B.; Abruna, H. D.; Coates, G. W. Phosphonium-Functionalized Polyethylene: A New Class of Base-Stable Alkaline Anion Exchange Membranes. *J. Am. Chem. Soc.* **2012**, *134*, 18161−18164.
(18) Zhang, S. H.; Zhang, B. G.; Xing, D. B.; Jian, X. G. Poly(Phthalazinone Ether Ketone Ketone) Anion Exchange Membranes with Pyridinium as Ion Exchange Groups for Vanadium Redox Flow Battery Applications. *J. Mater. Chem. A* **2013**, *1*, 12246−12254.
(19) Zhang, B. Z.; Gu, S.; Wang, J. H.; Liu, Y.; Herring, A. M.; Yan, Y. S. Tertiary Sulfonium as a Cationic Functional Group for Hydroxide Exchange Membranes. *R. Soc. Chem. Adv.* **2012**, *2*, 12683−12685.
(20) Deavin, O. I.; Murphy, S.; Ong, A. L.; Poynton, S. D.; Zeng, R.; Herman, H.; Varcoe, J. R. Anion-Exchange Membranes for Alkaline Polymer Electrolyte Fuel Cells: Comparison of Pendent Benzyltrimethylammonium- and Benzylmethylimidazolium-Head-Groups. *Energy Environ. Sci.* **2012**, *5*, 8584−8597.
(21) Guo, M. L.; Fang, J.; Xu, H. K.; Li, W.; Lu, X. H.; Lan, C. H.; Li, K. Y. Synthesis and Characterization of Novel Anion Exchange Membranes Based on Imidazolium-Type Ionic Liquid for Alkaline Fuel Cells. *J. Membr. Sci.* **2010**, *362*, 97−104.
(22) Wang, J. H.; Li, S. H.; Zhang, S. B. Novel Hydroxide-Conducting Polyelectrolyte Composed of an Poly(Arylene Ether Sulfone) Containing Pendant Quaternary Guanidinium Groups for Alkaline Fuel Cell Applications. *Macromolecules* **2010**, *43*, 3890−3896.
(23) Zha, Y. P.; Disabb-Miller, M. L.; Johnson, Z. D.; Hickner, M. A.; Tew, G. N. Metal-Cation-Based Anion Exchange Membranes. *J. Am. Chem. Soc.* **2012**, *134*, 4493−4496.
(24) Ye, Y.; Elabd, Y. A. Relative Chemical Stability of Imidazolium-Based Alkaline Anion Exchange Polymerized Ionic Liquids. *Macromolecules* **2011**, *44*, 8494−8503.
(25) Ran, J.; Wu, L.; Varcoe, J. R.; Ong, A. L.; Poynton, S. D.; Xu, T. Development of Imidazolium-Type Alkaline Anion Exchange Membranes for Fuel Cell Application. *J. Membr. Sci.* **2012**, *415*, 242−249.
(26) Awad, W. H.; Gilman, J. W.; Nyden, M.; Harris, R. H.; Sutto, T. E.; Callahan, J.; Trulove, P. C.; DeLong, H. C.; Fox, D. M. Thermal Degradation Studies of Alkyl-Imidazolium Salts and Their Application in Nanocomposites. *Thermochim. Acta* **2004**, *409*, 3−11.
(27) Lin, B. C.; Dong, H. L.; Li, Y. Y.; Si, Z. H.; Gu, F. L.; Yan, F. Alkaline Stable C2-Substituted Imidazolium-Based Anion-Exchange Membranes. *Chem. Mater.* **2013**, *25*, 1858−1867.
(28) Mamlouk, M.; Ocon, P.; Scott, K. Preparation and Characterization of Polybenzimidzaole/Diethylamine Hydrogen Sulphate for Medium Temperature Proton Exchange Membrane Fuel Cells. *J. Power Sources* **2014**, *245*, 915−926.
(29) Page, O. M. M.; Poynton, S. D.; Murphy, S.; Ong, A. L.; Hillman, D. M.; Hancock, C. A.; Hale, M. G.; Apperley, D. C.; Varcoe, J. R. The Alkali Stability of Radiation-Grafted Anion-Exchange Membranes Containing Pendent 1-Benzyl-2,3-Dimethylimidazolium Head-Groups. *RSC Adv.* **2013**, *3*, 579−587.
(30) Zhang, F. X.; Zhang, H. M.; Qu, C. Imidazolium Functionalized Polysulfone Anion Exchange Membrane for Fuel Cell Application. *J. Mater. Chem.* **2011**, *21*, 12744−12752.
(31) Thomas, O. D.; Soo, K. J. W. Y.; Peckham, T. J.; Kulkarni, M. P.; Holdcroft, S. A Stable Hydroxide-Conducting Polymer. *J. Am. Chem. Soc.* **2012**, *134*, 10753−10756.
(32) Tse, Y.-L. S.; Sarode, H. N.; Lindberg, G. E.; Witten, T. A.; Yang, Y.; Herring, A. M.; Voth, G. A. Chloride Enhances Fluoride Mobility in Anion Exchange Membrane/Polycationic Systems. *J. Phys. Chem. C* **2014**, *118*, 845−853.
(33) Wang, J. H.; Gu, S.; Kaspar, R. B.; Zhang, B. Z.; Yan, Y. S. Stabilizing the Imidazolium Cation in Hydroxide-Exchange Membranes for Fuel Cells. *ChemSusChem* **2013**, *6*, 2079−2082.
(34) Sheen, H. T.; Kahler, H. L. Effect of Ions on Mohr Method for Chloride Determination. *Ind. Eng. Chem., Anal. Ed.* **1938**, *10*, 628−629.
(35) Kang, M. S.; Choi, Y. J.; Moon, S. H. Water-Swollen Cation-Exchange Membranes Prepared Using Poly(Vinyl Alcohol) (PVA)/Poly(Styrene Sulfonic Acid-co-Maleic Acid) (Pssa-Ma). *J. Membr. Sci.* **2002**, *207*, 157−170.
(36) Liu, Y.; Horan, J. L.; Schlichting, G. J.; Caire, B. R.; Liberatore, M. W.; Hamrock, S. J.; Haugen, G. M.; Yandrasits, M. A.; Seifert, S.; Herring, A. M. A Small-Angle X-Ray Scattering Study of the Development of Morphology in Films Formed from the 3m Perfluorinated Sulfonic Acid Ionomer. *Macromolecules* **2012**, *45*, 7495−7503.
(37) Volkov, V. I.; Korotchkova, S. A.; Ohya, H.; Guo, Q. H. Self-Diffusioni of Water-Ethanol Mixtures in Polyacrylic-Acid Polysulfone Composite Membranes Obtained by Pulsed-Field Gradient Nuclear Gradient Nuclear-Magnetic-Resonance Spectroscopy. *J. Membr. Sci.* **1995**, *100*, 273−286.
(38) Volkov, V. I.; Popkov, Y. M.; Timashev, S. F.; Bessarabov, D. G.; Sanderson, R. D.; Twardowski, Z. Self-Diffusion of Water and Fluorine Ions in Anion-Exchange Polymeric Materials (Membranes and Resin) as Determined by Pulsed-Field Gradient Nuclear Magnetic Resonance Spectroscopy. *J. Membr. Sci.* **2000**, *180*, 1−13.
(39) Maes, A. M.; Pandey, T. P.; Vandiver, M. A.; Lundquist, L. K.; Yang, Y.; Horan, J. L.; Krosovsky, A.; Liberatore, M. W.; Seifert, S.;

Herring, A. M. Preparation and Characterization of an Alkaline Anion Exchange Membrane from Chlorinated Poly (Propylene) Aminated with Branched Poly (Ethyleneimine). *Electrochim. Acta* **2013**, *110*, 260−266.
(40) Li, W.; Fang, J.; Lv, M.; Chen, C.; Chi, X.; Yang, Y.; Zhang, Y. Novel Anion Exchange Membranes Based on Polymerizable Imidazolium Salt for Alkaline Fuel Cell Applications. *J. Mater. Chem.* **2011**, *21*, 11340−11346.
(41) Komkova, E. N.; Stamatialis, D. F.; Strathmann, H.; Wessling, M. Anion-Exchange Membranes Containing Diamines: Preparation and Stability in Alkaline Solution. *J. Membr. Sci.* **2004**, *244*, 25−34.
(42) Kroon, M. C.; Buijs, W.; Peters, C. J.; Witkamp, G.-J. Quantum Chemical Aided Prediction of the Thermal Decomposition Mechanisms and Temperatures of Ionic Liquids. *Thermochim. Acta* **2007**, *465*, 40−47.
(43) Lin, X.; Varcoe, J. R.; Poynton, S. D.; Liang, X.; Ong, A. L.; Ran, J.; Li, Y.; Xu, T. Alkaline Polymer Electrolytes Containing Pendant Dimethylimidazolium Groups for Alkaline Membrane Fuel Cells. *J. Mater. Chem. A* **2013**, *1*, 7262−7269.
(44) Garcia, R.; Perez, R. Dynamic Atomic Force Microscopy Methods. *Surf. Sci. Rep.* **2002**, *47*, 197−301.
(45) Canetti, M.; Bertini, F.; Scavia, G.; Porzio, W. Structural Investigation on Bulk Poly(3-Hexylthiophene): Combined Saxs, Waxd, and Afm Studies. *Eur. Polym. J.* **2009**, *45*, 2572−2579.
(46) Schnablegger, H.; Singh, Y. *The SAXS Guide—Getting Acquainted with the Principles*; Anton Paar GmbH: Austria, 2011.
(47) Hashimoto, T.; Shibayama, M.; Kawai, H. Domain-Boundary Structure of Styrene-Isoprene Block Co-Polymer Films Cast from Solution 0.4. Molecular-Weight Dependence of Lamellar Microdomains. *Macromolecules* **1980**, *13*, 1237−1247.
(48) Cho, C. H.; Hong, Y. S.; Kang, K.; Volkov, V. I.; Skirda, V.; Lee, C. Y. J.; Lee, C. H. Water Self-Diffusion in Chlorella Sp Studied by Pulse Field Gradient Nmr. *Magn. Reson. Imaging* **2003**, *21*, 1009−1017.
(49) Janarthanan, R.; Horan, J. L.; Caire, B. R.; Ziegler, Z. C.; Yang, Y.; Zuo, X.; Liberatore, M. W.; Hibbs, M. R.; Herring, A. M. Understanding Anion Transport in an Aminated Trimethyl Polyphenylene with High Anionic Conductivity. *J. Polym. Sci., Part B* **2013**, *51*, 1743−1750.
(50) Wende, C.; Schonhoff, M. Dynamics of Water in Polyelectrolyte Multilayers: Restricted Diffusion and Cross-Relaxation. *Langmuir* **2010**, *26*, 8352−8357.
(51) Rollet, A. L.; Simonin, J. P.; Turq, P.; Gebel, G.; Kahn, R.; Vandais, A.; Noel, J. P.; Malveau, C.; Canet, D. Self-Diffusion of Ions at Different Time Scales in a Porous and Charged Medium: The Nafion Membrane. *J. Phys. Chem. B* **2001**, *105*, 4503−4509.
(52) Liu, Y.; Sambasivarao, S. V.; Horan, L. J.; Yang, Y.; Maupin, M. C.; Herring, A. M. A Combined Theoretical and Experimental Investigation of the Transport Properties of Water in a Perfluorosulfonic Acid Proton Exchange Membrane Doped with the Heteropoly Acids, H3pw12o40 or H4siw12o40. *J. Phys. Chem. C* **2014**, *118*, 854−863.
(53) A Latour, L. L.; Mitra, P. P.; Kleinberg, R. L.; Sotak, C. H. Time-Dependent Diffusion Coefficient of Fluids in Porous Media as a Probe of Surface-to-Volume Ratio. *J. Magn. Reson., Ser. A* **1993**, *101*, 342−346.
(54) Hou, J. B.; Li, J.; Mountz, D.; Hull, M.; Madsen, L. A. Correlating Morphology, Proton Conductivity, and Water Transport in Polyelectrolyte-Fluoropolymer Blend Membranes. *J. Membr. Sci.* **2013**, *448*, 292−299.
(55) Slade, R. C. T.; Varcoe, J. R. Investigations of Conductivity in Fep-Based Radiation-Grafted Alkaline Anion-Exchange Membranes. *Solid State Ionics* **2005**, *176*, 585−597.
(56) Santasalo-Aarnio, A.; Hietala, S.; Rauhala, T.; Kallio, T. In and Ex Situ Characterization of an Anion-Exchange Membrane for Alkaline Direct Methanol Fuel Cell (Admfc). *J. Power Sources* **2011**, *196*, 6153−6159.
(57) McIntosh, L. D.; Kubo, T.; Lodge, T. P. Morphology, Modulus, and Conductivity of a Triblock Terpolymer/Ionic Liquid Electrolyte Membrane. *Macromolecules* **2014**, *47*, 1090−1098.
(58) Ye, Y.; Elabd, Y. A. Anion Exchanged Polymerized Ionic Liquids: High Free Volume Single Ion Conductors. *Polymer* **2011**, *52*, 1309−1317.
(59) Karger, N.; Vardag, T.; Ludemann, H. D. Temperature-Dependence of Self-Diffusion in Compressed Monohydric Alcohols. *J. Chem. Phys.* **1990**, *93*, 3437−3444.
(60) Pendzig, P.; Dieterich, W.; Nitzan, A. Monte Carlo Study of Diffusion in Polymer Electrolytes. *J. Non-Cryst. Solids* **1998**, *235*, 748−752.
(61) Ratner, M. A. Aspects of the Theoretical Treatment of Polymer Solid Electrolytes: Transport Theory and Models. *Polymer Electrolyte Reviews* **1987**, *1*, 173−236.
(62) Cowie, J. M. G.; Martin, A.; Firth, A. M. Ionic Conductivity in Mixtures of Salts with Comb-Shaped Polymers Based on Ethylene Oxide Macromers. *Br. Polym. J.* **1988**, *20*, 247−252.